BMC Cancer

RESEARCH

Open Access

Zapotin mitigates breast cancer progression by targeting PKCε mediated glycolytic pathway regulation

Khushbukhat Khan[1], Maryam Anwar[1], Yasmin Badshah[1], Naeem Mahmood Ashraf[2*], Arslan Hamid[3], Janeen H. Trembley[4,5,6], Maria Shabbir[1], Tayyaba Afsar[7], Fohad Mabood Husain[8], Dilawar Khan[1] and Suhail Razak[7*]

Abstract

Background The breast cancer recurrence and chemoresistance has increased over the years. A novel PKC, PKCε, may promote chemoresistance by causing hypoxia and cancer metabolic rewiring. A natural flavonoid, Zapotin, in colon cancer cells may modulate PKCε expression. Therefore, this study aimed to explore Zapotin impact on PKCε expression and the metabolic profile of breast cancer cells.

Methods Pharmacophore analysis of Zapotin was performed and molecular dynamics (MD) simulations were employed to study PKCε and Zapotin interaction stability. The effect of Zapotin treatment on PKCε expression and various aspects of cancer cell viability and metabolism was studied in MCF-7 and MDA-MB-231 breast cancer cell lines using real-time PCR, growth and death assays, and Gas Chromatography-Mass Spectrometry.

Results In silico analyses revealed good solubility and absorption of Zapotin with lower toxicity. Zapotin showed cancer cell-specific cytotoxicity ($P < 0.0001$). It's treatment also reduced breast cancer cell viability, colony formation, and migratory potential by targeting PKCε and associated HIF-1α and VEGF signaling ($P < 0.01$). Zapotin also impacted PKCε-mediated metabolic signaling by targeting glycolytic pathways.

Conclusion This study demonstrated the role of PKCε mediated HIF-1α, VEGF, and glycolytic pathways in promoting breast carcinogenicity and demonstrated Zapotin as a potential treatment option for different types of breast tumors.

Keywords Protein kinase C epsilon, Zapotin, MD simulations, Breast cancer, Metabolic rewiring

*Correspondence:
Naeem Mahmood Ashraf
naeem.sbb@pu.edu.pk
Suhail Razak
smarazi@ksu.edu.sa
[1]Department of Biomedicine, Atta-ur-Rahman School of Applied Biosciences (ASAB), National University of Sciences and Technology (NUST), Islamabad 44000, Pakistan
[2]School of Biochemistry & Biotechnology, University of the Punjab, Lahore, Pakistan
[3]LIMES Institute (AG-Netea), University of Bonn, Carl-Troll-Str. 31, 53115 Bonn, Germany
[4]Department of Laboratory Medicine and Pathology, University of Minnesota, Minneapolis, MN, USA
[5]Masonic Cancer Center, University of Minnesota, Minneapolis, MN, USA
[6]Minneapolis VA Health Care System Research Service, Minneapolis, MN, USA
[7]Department of Community Health Sciences, College of Applied Medical Sciences, King Saud University, Riyadh, Saudi Arabia
[8]Department of Food Science and Nutrition, College of Food and Agriculture Sciences, King Saud University, Riyadh, Saudi Arabia

Background

Recent data demonstrate a rise in breast cancer incidence and associated mortality worldwide. Approximately 313,510 new breast cancer cases are estimated in the United States alone in 2024. Among these, 42,780 lives are estimated to be claimed by breast carcinoma [1, 2]. Globally, breast cancer accounts for ~12% of cancers diagnosed in females. Worldwide statistics reported 2 million newly diagnosed breast cancer cases in 2018 [3, 4].

Increased knowledge of the molecular pathology of breast cancer and advancement in high-throughput technology contributed to increased five-year survival in breast cancer [5]. Despite improved strategies for early screening and better disease management, drug resistance and cancer recurrence remain major obstacles in treating breast cancer [6, 7]. Identification of molecular markers is needed to overcome improved breast cancer prognosis, develop new treatments, and decrease breast cancer-related mortality [8–11].

Protein kinase C epsilon (PKCε) belongs to the novel protein kinase C family class. Its association with all cancer hallmarks including growth inhibitory signal evasion, apoptosis resistance, replicative immortality, angiogenesis, immune escape, and invasion and metastasis has been reported in different cancers [12–16]. Furthermore, aberrant PKCε expression is associated with the emergence of drug resistance in cancers. Mechanistically, PKCε promotes the expression of a multidrug-resistant (MDR/ABCB1) gene that causes the efflux of therapeutic agents from cancer cells, rendering them resistant to therapy [17, 18].

Literature has also indicated PKC family protein's role in modulating the activity of Akt that also contributes to carcinogenicity [19]. Conventional PKC-beta is reported to activated Akt in response to glucose [20]. However, no experimental evidence ever demonstrated the contribution of PKCε in mediating breast carcinogenicity by modulating Akt pathway. Evidence also suggest PKCε's role in modulating insulin metabolism and glucose metabolism [21, 22]. However, studies indicating PKCε contribution in promoting metabolic alteration in cancer are scarce.

Its role in modulating hypoxia in several cardiac anomalies has also been reported. PKCε has been reported to sooth hypobaric hypoxia in mouse by inhibiting GSK3β/HIF-1α expression and regulating glucose utilization in cardiac mitochondria [23]. However, in another study, PKCε inhibition or gene silencing was found to lower hypoxia in pulmonary artery smooth muscle cell [24]. In cancer, PKCε's contribution in hypoxia is not fully explored.

In vitro, inhibition of PKCε is demonstrated to block these cancer hallmark activities and restore sensitivity to chemo- and radio-therapies [13, 25–28]. The natural flavonoid 5,6,2',6'- tetramethoxyflavone (Zapotin) is present in zapote blanco (a tropical fruit) and is reported to have anti-cancer activity [29, 30]. It is studied for its antidepressant, anti-oxidative, anticonvulsant, anti-microbial, and anti-fungal properties [31]. It is also evaluated for its anti-cancer properties in HeLa cell lines and skin cancer animal model [32, 33]. Studies in colon cancer cell lines and xenografted mice revealed that Zapotin treatment induces apoptosis and reduces colon carcinogenicity [34]. In addition, Zapotin modulates PKCε signaling to induce programmed cell death in HeLa cells [29]. However, anti-carcinogenic influence of Zapotin in breast cancer have never been explored. Studies also lack evidence on delineating PKCε's role in metabolic alteration in breast cancer. Therefore, in the present study, we coupled bioinformatics, molecular biology, and analytical techniques to determine the influence of Zapotin on PKCε expression and understand its impact on the metabolic profile of breast cancer cells. This is the first study to delineate strong molecular interaction between PKCε and Zapotin and suggested Zapotin as a new potent therapeutic option for treating invasive breast cancer by targeting PKCε. Furthermore, this study also provided evidence for PKCε as a key contributor in metabolic rewiring in breast cancer.

Methods

The tertiary structure of PKCε was previously predicted [35] using a threading approach [36] and validated through ERRAT analysis, Ramachandran plot analysis, and alignment analysis [37]. The stability of the predicted structure was also evaluated through molecular dynamics (MD) simulations [35]. The current study employed a similar structure to determine molecular interaction stability between Zapotin and PKCε. All methods were performed in accordance with the relevant guidelines and regulations.

Localization prediction of PKCε

PKCε sub-cellular localization was predicted through deep learning tools DeepLoc1.0 (https://services.healthtech.dtu.dk/services/DeepLoc-1.0/ [38]), and TMHMM2.0 (https://services.healthtech.dtu.dk/services/TMHMM-2.0/ [39]),. Further, the presence of signal sequences for secretion and organelle translocation (mitochondria/endoplasmic reticulum/Golgi apparatus) was investigated through SignalP-5.0 (https://services.healthtech.dtu.dk/services/SignalP-5.0/ [40]),, SecretomeP 1.0 (https://services.healthtech.dtu.dk/services/SecretomeP-1.0/ [41]),, and TargetP (https://services.healthtech.dtu.dk/services/TargetP-2.0/ [42]),. The prediction was based on the likelihood score obtained from each tool.

In silico pharmacophore analysis

LigandScout was employed to generate a pharmacophore model of Zapotin [43]. Web-based and standalone in-silico pharmacokinetics tools were applied to estimate the absorption, metabolism, distribution, and toxicity of 5,6,2',6'-Zapotin. A canonical simplified molecular input line entry (SMILE) system was employed to submit chemical structures in each software.

Algorithms on molinspiration (http://www.molinspiration.com/ [44]), admetSAR2.0 (http://www.admetexp.org [45]), OSIRIS property explorer (www.organic-chemistry.org/prog.pro [46]), VirtualRat (https://virtualrat.cmdm.tw/ [47]), ADVERPred (http://www.way2drug.com/adverpred/ [48]), and swissADME (http://www.swissadme.ch/index.php [49]), were performed. Physiochemical properties of the drug based on Lipinski rule and drug likeliness were estimated through molinspiration, admetSAR, 2.0, organic chemistry portal, virtual rat, and swissADME. Scores from admetSAR2.0, molinspiration, VirtualRat, ADVERPred, and swissADME were employed to predict ADME parameters, pharmacokinetic and toxicological properties, including carcinogenicity, mutagenicity, and adverse effects. The bioactivity of the drug was estimated through molinspiration and admetSAR2.0.

Molecular docking

PubChem database was used to retrieve the structure of the ligand Zapotin (Compound CID: 629965). The energy of the downloaded structure was minimized through chemdraw 2016 (PerkinElmer, Inc, Waltham, MA 02451 USA). CB-dock webserver was employed for the docking of PKCε with energy-minimized Zapotin. This webserver uses a curvature-based cavity detection approach, and the Autodock Vina program was applied to predict the binding modes. Based on the Vina score and cavity size, the selection of binding mode is done (http://clab.labshare.cn/cb-dock/ [50]),. Visualization and analysis of electrostatic and non-electrostatic interactions were performed through LigPlot^{+} version 2.2 [51].

Molecular dynamics simulations (MD simulation)

The Zapotin-PKCε complex was simulated for 10ns using GROMACS on a Linux platform [52]. The ligand's topology was generated using the CGenFF server, while the CHARMM26 force field was employed for the protein's topology. The water box filled with TIP3P water molecules, complemented with sodium and chloride ions, was used for solvation. Following a 200 ps steepest descent energy minimization, the system underwent equilibration for volume, pressure, and temperature. The 100ns MD production was then executed. The trajectory was constructed using the gmx_ trjconv command for the post-simulation analysis. The built-in GROMACS commands: gmx rms, gmx rmsf, gmx area, and gmx cod, were used for calculating Root Mean Square Deviation (RMSD), Root Mean Square Fluctuation (RMSF), Solvent Accessible Surface Area (SASA), and the count of hydrogen bonds.

Cell culture and maintenance

Human breast cancer MDA-MB-231 and MCF-7 cell lines were obtained from ATCC and cultured in Roswell Park Memorial Institute Medium (RPMI) (Gibco, Life Technologies), supplemented with 10% fetal bovine serum (FBS) (Gibco, Life Technologies) and 1% penicillin-streptomycin (Gibco, Life Technologies) in an incubator provided with 5% carbon dioxide at 37 °C. Cell harvesting was performed with trypsin-EDTA.

Cytotoxicity assay

Zapotin was purchased from Sigma-Aldrich (LOT # 65548-55-2). Assessment of Zapotin treatment on cell viability was performed using MTT (3-(4,5-dimethyl thiazol-2yl)-2,5-diphenyl tetrazolium bromide) assay (Mosmann, 1983). MDA-MB-231 and MCF-7 cells were plated in 96-well plates (7000 cells/well) in 200 µl of growth medium. Dose-dependent cytotoxic influence of Zapotin was studied by treating plated cells with varying drug concentrations (ranging from 0.15 to 0.35 µM). The dose range was selected by testing different dosages from 0 µM to 0.35 µM (Supplementary file S Table 2). After 48 h of incubation, media was aspirated, and cells were subjected to 1X PBS washing. Serum-free media diluted-MTT (100 µl) was added in each well and, as a solubilization solution, further incubated for 2 h at 37 °C in a humidified atmosphere. DMSO (100 µl) was added as a solubilization solution for formazan, and formazan concentration was measured at 550 wavelength. Percentage cell viability is calculated through.

$$\%\text{Cell Viability} = \frac{\text{Absorbance of Control Wells}}{\text{Absorbance of Treated Wells}} \times 100$$

The significance is determined through one-way ANOVA and each experiment was repeated in triplicates.

Wound healing assay

Breast cancer cells were seeded in cell culture plates and allowed to achieve 70–80% confluency. After 24 h of incubation, the medium was removed, and sterile 2-mm wide pipette tips were used to scrape and create a gap of constant width in the monolayer. The wounded monolayer was subjected to PBS washing to remove cell debris, and cells were subsequently exposed to various concentrations of drug or DMSO alone. Cell movement for the next 24 h was photographed at regular intervals using LSM 410 microscope (Zeiss, Germany).

Colony formation assay

Zapotin treatment effect on the colony formation potential of breast cancer cells was assessed through a clonogenic assay. MDA-MB-231 and MCF-7 cells were seeded (density 1000 cells/well) in 12-well plates in triplicate. After 24 h, the medium was substituted with media containing different drug concentrations. Media with floating cells from wells was collected after 48 h, spun for 3 min at 1500 x rpm, and the pellet was collected. Cells were resuspended in fresh medium, replating in a 12-well plate, and incubated in a 5% CO_2-humidified atmosphere for 2 weeks. Fresh media was added every 4 days, and regular observation under the microscope was done for colony formation. After 2 weeks, media was removed, and cells stained with a staining solution (0.5% crystal violet prepared in glacial acetic acid, methanol, and distilled water) for 45 min. After PBS wash, pictures of the colonies were taken.

Cell staining and flow cytometry

The collection of cells was carried out by centrifuging them at 800 rpm and washed with 1X PBS. The supernatant was removed, and 1X FBS (500 µl) and Annexin V binding buffer (100 µl) was utilized for resuspending ~ 1×10^6 cells. After incubation at room temperature for 5 min, centrifugation for 5 min at 400 rpm was performed.

Cells were subjected to suspension in dyes Annexin V (5 µl) and propidium iodide (5 µl), along with Annexin V binding buffer (1X, 100 µl), and spun gently for homogeneous mixing. The resultant mixture was incubated in the dark at room temperature for 20 min. After incubation, binding buffer (1X, 400 µl) was added, and unbound dye was removed by centrifugation in the tube. Stained cells were immediately assessed by flow cytometry. Healthy cells will be Annexin V and propidium iodide negative. Late apoptotic cells will be Annexin V and propidium iodide positive, whereas early apoptotic cells will be Annexin V positive and propidium iodide negative. The experiment was repeated twice.

Real-time PCR

Pallets of MCF-7 and MDA-MB-231 cells were collected after 24 h of Zapotin treatment, and extraction of RNA was performed through the TriZol method as described [53], with few modifications. After adding TriZol and chloroform in cell pellet, the solution was hand mixed for 1 min and centrifuges for 15 min. Rest of the protocol for followed as described in [53]. The complementary DNA (cDNA) was synthesized using > 1 µg of RNA template. Solice BioDyn cDNA synthesis kit (Tartu, Estonia) was used for cDNA synthesis, and the procedure was carried out per the manufacturer's instructions. A reaction mixture of 20 µl total volume was prepared by adding 10 µg cDNA, 1 µl forward and reverse primers, 10 µl PowerUp™ SYBR™ Green Master Mix (Thermofisher Scientific, United States), and nuclease-free water. Amplification and real-time conditions were: initial denaturation for 2 min at 95°C, then 40 cycles of denaturation at 95°C for 30 s, amplification at 61°C for 15 s, and real-time analysis. The reaction was carried out on Applied Biosystems 7300 Real-Time PCR System, and data analysis was performed through the system's SDs software. Normalization was performed using beta-actin primers, and expression quantification was done through the double-CT (2^(-ΔΔ) CT) method [54]. The expression of PKCε was studied along with SOCS3, AKT, VEGF, and HIF-1α to analyze the impact of Zapotin on its upstream and downstream targets. The primer sequences are:

PKCε

Forward *5'AGCCTCGTTCACGGTTCT3'.*
Reverse *5'TGTCCAGCCATCATCTCG3'.*

HIF1α

Forward *5'CAGATCTCGGCGAAGTAAAG3'.*
Reverse *5'TCACAGAGGCCTTATCAAGATG3'.*

SOC3

Forward *5'CACCTGGACTCCTATGAGAAAGTCA3.*
Reverse *5'GGGGCATCGTACTGGTCCAGGAA3'.*

VEGF

Forward *5'CGAGGGCCTGGAGTGTG3'.*
Reverse *5'CCGCATAATCTGCATGGTGAT3'.*

AKT

Forward *5'TTCTGCAGCTATGCGAATCTC3'.*
Reverse *5'TGGCCAGCATACCATAGTGAGGTT3'.*

Beta-actin

Forward *5'CACCATTGGCAATGAGCGGTTC3'.*
Reverse *5'AGGTCTTTGCGGATGTCCACGT3'.*

Statistical analysis

A double delta method was used for the calculation of fold change [55]. Experiment was repeated in triplicate and the association between target genes' expression with Zapotin treatment was determined through One-way ANOVA. All analysis was computed through Graphpad Prism 8.0.1 (GraphPad Software Inc., San Diego, CA, USA). P-value less than 0.05 depicted significance.

Gas chromatography coupled with mass spectrometry (GC-MS)

Breast cancer cell pellets representing Zapotin treated and untreated conditions in triplicate (MCF-7 and MDA-MB-231) were suspended in PBS and collected in 2 ml

microcentrifuge vials. All samples were centrifuged at 13000xg for 5 min at 4 °C, the supernatant was collected, and roughly 3 million cells were subjected to sample preparation for metabolome analysis. The protocol for GC-MS sample preparation and analysis was as described by Semreen et al., 2019 [56] with slight modifications.

Sample preparation

Methanol (0.1% v/v, Sigma Aldrich, Massachusetts, United States) was added to pellets and vortexed for 5 min. Samples were incubated on ice for one hour, during which each sample was subjected to brief vortex mixing every 10 min. Centrifugation was carried out for 10 min at 13,000 rpm to separate the cell insoluble matrix, and the supernatant was taken in GC vials. The supernatant was dried at 37 °C in Eppendorf Vacufuge® Vacuum Concentrator (Eppendorf, United Kingdoms) [56]. The dried samples were then dissolved in 50 µl of a solution (methoxyamine hydrochloride (Sigma Aldrich, Massachusetts, United States) in pyridine (20 mg/ml, Sigma Aldrich, Massachusetts, United States)). Then, a solution consisting of MSTFA (Sigma Aldrich, Massachusetts, United States) and 1% TMCS (25 µl, Sigma Aldrich, Massachusetts, United States) was added along with pyridine (100 µl). Samples were subjected to 30 min of incubation at 50 °C to ensure complete derivatization and were then immediately transferred to the instrument's microinserts.

GC-MS analysis

Metabolic analysis was performed in GC/MS-QP 2010 Ultra System (Shimadzu, Kyoto, Japan) with LabSolutions GC-MS software (v1.20). The metabolite separation was performed through a Restek Rtx® – 5ms column (30.0 m × 0.25 mm, 0.25 µm), where Helium (99.9%) was used as the carrier gas (flow rate 1.0 ml/min). The oven's initial temperature was at 60 °C, held for 2 min, raised to 310 °C by 5 °C/min, and held during the analysis. The auxiliary temperatures: ionization and interface, were set at 250 °C. Metabolite analysis was carried out in full scan mode. Auto-injector AOC-20i (Shimadzu, Kyoto, Japan) was utilized for injecting 10 µl of sample in splitless mode. NIST/EPA/NIH Mass Spectral Library (NIST 14) was utilized to identify total ion chromatograms (TIC) and metabolites' fragmentation patterns. For each sample, the run time opted was approximately 44 min.

GC-MS data analysis

The manual filtration technique opted for removing unidentified ions from the data table. As the experiment was conducted in triplicates, mean for each metabolite data was taken. The normalization of the data was based on the total peak height, and the signals belonging to the similar ion category were put in the same group. The resultant metabolic data table was then analyzed thoroughly [56].

Before commencing analysis, the KEGG IDs of the compounds were obtained from the KEGG compound database [57] and similar metabolites in treated and untreated groups were selected. Based on area and height, quantification of metabolites was performed, and fold change was measured [58]. Identifying significantly altered metabolites in response to drug treatment was performed through a student t-test where the significance threshold was less than 0.05. To reduce the probability of false positive identification, the false discovery rate (FDR) was set below 5% and calculated through the q-conversion algorithm [59]. The PCA plot was constructed using the "prcomp" function from basic R-packages. The analysis relied on the "stats" library for the prcomp function and the "ggplot2" package for PCA visualization.

Functional metabolomics analysis

Metabolic coverage between the treated and untreated samples was performed using network-based metabolic pathway analysis (MPA) and MSEA [60]. Furthermore, the associated genes with these pathways were also obtained through the Cytoscape v3.8.2 program [61] and Ingenuity Pathway Analysis (IPA) tool. The genes were further distributed into different categories based on their molecular, biological, and functional properties by Protein Analysis Through Evolutionary Relationships (PANTHER; http://www.pantherdb.org/ [62]) and Gene Ontology database [63].

Cell pathway construction

Construction of cellular pathways depicting possible PKCε molecular interactions was performed through Ingenuity Pathway Analysis Software (QIAGEN Inc [64]). Information for protein-protein networks as well as canonical pathways, was gathered by providing metabolites as inputs and utilizing log2 fold-change, FDR, and p-values.

Results

Localization of *PKCε*

Signal sequence analysis revealed that PKCε does not contain a signal peptide, secretion signal peptide, or mitochondrial transfer peptide, suggesting PKCε is not a secretory protein (Table 1). Subcellular localization analysis showed that PKCε does not localize to any organelle. Based on a cytoplasmic localization score of 0.9078 and a solubility score of 0.8, it is determined that PKCε is a soluble cytoplasmic protein (Fig. 1).

In silico pharmacokinetic evaluation of Zapotin

The Pharmacophore model of Zapotin was generated through LigandScout and revealed three aromatic rings,

Table 1 Likelihood score for PRKCE extracellular and subcellular localization

Signal sequences	**SignalP-5.0**		**SecretomeP 1.0**		**TargetP**	
	Likelihood	**Other**	**Likelihood**	**Other**	**Likelihood**	**Other**
Mitochondrial transfer peptide	0.0682	0.9292	.	.	.	.
Secretion signal Peptide	.	.	0.325	0.611	.	.
Signal Peptide	0.0026	.	.	.	0.004	0.996
Subcellular localization	**DeepLoc1.0**	**TMHMM2**	**Type**	**Score**		
Nucleus	0.0866	.	**Soluble**	0.998		
Cytoplasm	0.9078	.	**Membrane**	0.002		
Cell membrane	0.0011	0.00006				
Endoplasmic reticulum	0.0002	.				
Golgi apparatus	0.0002	.				
Peroxisomes	0.0009	.				
Extracellular	0.0005	.				

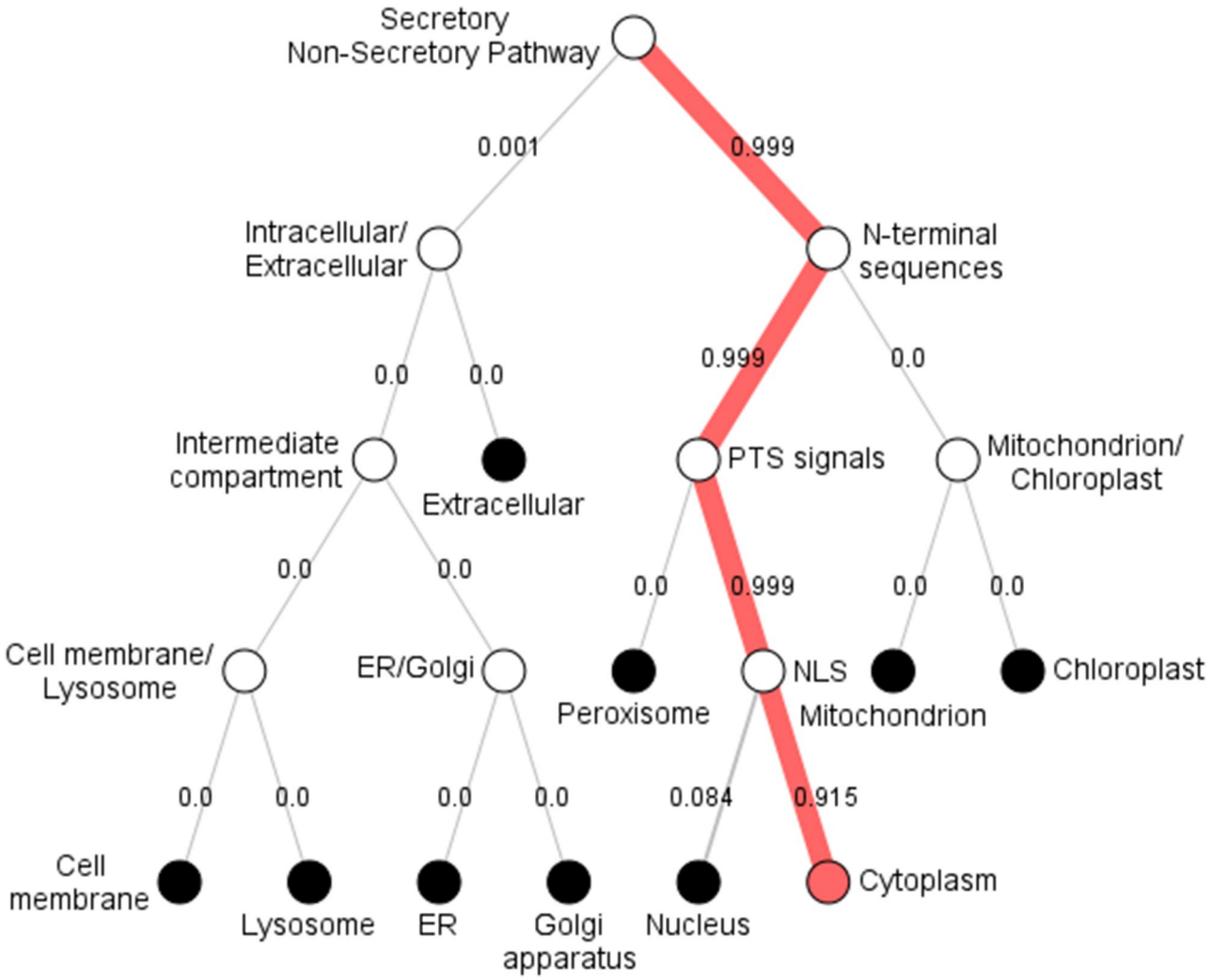

Fig. 1 Subcellular localization of PKCε: DeepLoc score indicated a high probability of cytoplasmic localization of PKCε. Empty circles indicate a continued pathway. Black circles show the destination. The orange circle shows the final destination of the protein

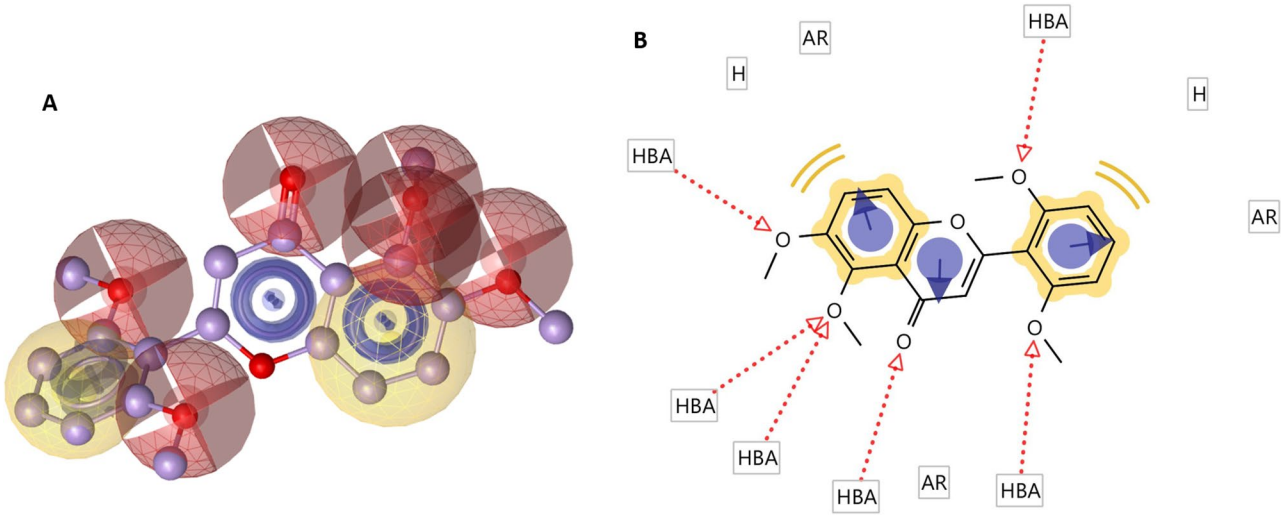

Fig. 2 Pharmacophore model of Zapotin: **A**) Three-dimensional representation of Zapotin ligand model. Red spheres depict hydrogen bond donors, yellow spheres indicate hydrophobic region, and purple spheres represent aromatic rings. **B**) Two-dimensional representations of the Zapotin ligand model and the same color theme with the same descriptors are used. **Abbreviations**: H: Hydrogen bonds, AR: Aromatic rings, HBA: Hydrogen bonds acceptor

Table 2 List of different properties of Zapotin and respective score predicted by molinspiration, admetsar, organic chemistry portal, virtual rat and SwissADME

Property		**Value**				
		Molinspiration	**admetSAR 2.0**	**OSIRIS**	**VirtualRat**	**SwissADME**
Sr no	**Lipinski rule of 5**					
1	Molecular weight (g/mol)	342.35	342.35	342	342.110	342.34
2	H-bond donor	0	0	-	0	0
3	H-bond acceptor	6	6	-	6	6
4	MLogP	3.57	3.49	3.09	3.49	3.39
	Violations	**0**	**0**	**-**	**-**	**0**
5	Rotatable bonds	5	5	-	-	5
6	TPSA (Å)	67.15	-	63.22	67.130	67.13
7	Druglikeness	-	-	-0.23	-	Yes
8	Drug score	-	-	0.56	-	-
9	LogS (solubility)	-	-3.867	-3.82	-	-4.04
10	Synthetic accessibility	-	-	-	-	3.62

two hydrophobic regions, and six hydrogen bond acceptor sites. Two-dimensional and three-dimensional models of the ligand are represented in Fig. 2.

Lipinski's rule of five estimates the permeation and absorption of the lead compound. Properties consisting of >500 Da molecular mass, 10 hydrogen bond acceptor number, >5 hydrogen bond donors number, and >5 CLogP (calculated LogP) value or >4.15 MLogP represent a high probability of poor absorption and permeation of the drug [65]. All tools predicted approximately 342 g/mol molecular weight, 0 hydrogen bond donors, 6 hydrogen bond acceptors, and <3.6 MLogP and agree with Lipinski's rules for small molecule therapeutics. Applied in silico pharmacokinetics tools (Molinspiration, admetSAR2.0, OSIRIS, VirtualRat, and SwissADME) estimated zero violations of Lipinski's rule (Table 2). LogP value estimated its moderate lipophilicity while LogS value (<-4) depicted its moderate aqueous solubility.

Total polar surface area (TPSA) and rotatable bonds less than 140 Å and 10, respectively, depict more probability of good drug bioavailability [66]. Analysis of the physicochemical properties of Zapotin indicated 5 rotatable bonds and TPSA less than 70 Å, estimating its good bioavailability (Table 2). SwissADME also predicted the synthetic accessibility (SA) of Zapotin. A higher SA score (10) represents greater difficulty in the mass synthesis of the lead compound. SA score of 3.42 estimated the ease of Zapotin synthesis at a large scale [67].

Drug pharmacokinetics include absorption, body distribution, metabolism, and excretion. admetSAR 2.0 and swissADME predicted high intestinal absorption of Zapotin. Similarly, scores from admetSAR and swissADME also indicated that the drug could penetrate

Table 3 Pharmacokinetics of Zapotin predicted by molinspiration, admetsar and virtual rat and SwissADME

Bioactivity	Score			
	Molinspiration	admetSAR 2.0	VirtualRat	SwissADME
Absorption				
Intestinal absorption	-	0.9928	-	High
Blood brain barrier	-	-0.2867	-0.02	Yes
Oral bioavailability	-	0.6857	-	0.55
Volume score*	302.18	-	-	-
Skin permeation (cm/s)	-	-	-	-6.21
Caco-2 permeability	-	0.8836	High	-
P-glycoprotein inhibitior	-	0.9397	Yes	-
P-glycoprotein substrate	-	-0.7987	No	No
Distribution and Metabolism				
Plasma protein binding (100%)	-	0.857	-	-
CYP450 substrate				
CYP3A4 substrate	-	-0.5097	-	-
CYP2C9 substrate	-	-1.0000	-	-
CYP2D6 substrate	-	-0.7654	-	-
CYP450 inhibitor				
CYP3A4 inhibition	-	0.6138	No	Yes
CYP2C9 inhibition	-	-0.7985	No	Yes
CYP2C19 inhibition	-	0.7445	Yes	Yes
CYP2D6 inhibition	-	-0.9546	No	Yes
CYP1A2 inhibition	-	0.9694	Yes	Yes
CYP inhibitory promiscuity	-	0.8123	-	-

*Molecular volume score predicted by Molinspiration depicts human absorption of ligand in intestine and brain

Caco-2 cells with high likelihood. Zapotin oral bioavailability is also predicted. VirtualRat and admetSAR anticipated lower transport of Zapotin across the blood-brain barrier (Table 3). AdmetSAR results suggested less likely binding of Zapotin with plasma protein (0.8%), further strengthening its stability and bioavailability. In silico pharmacokinetics analysis further indicated that Zapotin inhibits a few isoforms of CYP450 that might hinder the metabolism of co-administered drugs and result in drug accumulation-induced toxicity [68, 69].

Table 4 Bioactivity of Zapotin predicted by molinspiration and admetSAR

Bioactivity	Score	
	Molinspiration	admetSAR*
Kinase inhibitor	0.10	-
Nuclear receptor ligand	0.15	-
Enzyme inhibitor	0.10	-
Estrogen receptor binding	-	0.9178
Androgen receptor binding	-	0.8070
Thyroid receptor binding	-	0.7336
Glucocorticoid receptor binding	-	0.8812
Aromatase binding	-	0.7377

*High likelihood of certain event in admetSAR is estimated if obtained score is positive and near 1

A molinspiration bioactivity score falling in the range of 0–0.5 indicates moderate activity, while a score below 0.5 and above 0 depicts inactivity and high activity, respectively. These scores show lead compound likeliness properties. Molinspiration outcomes indicated Zapotin's high likeliness as an inhibitor of kinases (score 0.10) and enzymes (0.10) and as an interacting molecule for nuclear receptor ligand (0.15). AdmetSAR scores further elucidated the likeliness of Zapotin binding with nuclear receptors, including estrogen, androgen, thyroid, and glucocorticoid receptors. Zapotin is also estimated to have aromatase binding properties, a key enzyme in the estrogen synthesis pathway (Table 4).

Toxicity profiles obtained from admetSAR, OSIRIS, VirtualRat, and ADVERPred estimated lower toxicity of Zapotin. However, hepatic toxicity and arrhythmia (hERT inhibition) is predicted by admetSAR and ADVERPred. ADVERPred uses a PASS training set, and the estimation of drug toxicity is based on a comparison of values Pa (probability to be active) or Pi (probability to be inactive). Pa for hepatic toxicity and Human either-a-go-go (hERT) inhibition was more than Pi. The toxicity profile retrieved through in silico pharmacokinetics tools for Zapotin is listed in Table 5. The risk for mutagenesis and carcinogenicity is also estimated to be lower. Its acute oral toxicity is predicted to be 2.584 kg/mol, indicating the safety of oral administration of Zapotin.

Computation pharmacokinetics analysis indicated good solubility characteristics and good absorption of Zapotin. AdmetSAR, swissADME, and VirtualRat further estimated the high bioavailability of Zapotin with less assumed toxicity. However, its high ingestion might bring about arrhythmia and hepatic toxicity.

Molecular interaction between PKCε and Zapotin

A rigid docking approach opted for the molecular docking of PKCε with Zapotin through the CB-dock server. Five different binding conformations of the ligand-receptor interactions were obtained. Among these complexes, the selection for the best-docked model was based on

Table 5 Toxicity and adverse effects prediction of Zapotin by admetsar

Toxicity	Score			
	admetSAR	OSIRIS	VirtualRat	ADVERPred (Pa > Pi)
Acute oral toxicity	2.584 kg/mol	-	-	-
Hepatotoxicity	0.8750	-	-	0.413 > 0.249
Mutagenesis	0.5300	0	0	-
Carcinogenicity	-0.9173	0	0	-
Irritant	-	0	-	-
Eye irritation	0.7238		-	-
Eye corrosion	-0.9682			
Reproductive effect	-	0	-	-
Human either-a-go-go (hERT) inhibition	0.7091	-	Yes	0.324 > 0.265
Tetrahymena pyriformis toxicity	0.447 ug/L	-	-	-
Genotoxicity	0.7759	-	-	-

vina score and cavity size, as both parameters are indicators of stable protein and ligand binding. The model with the largest cavity size and lowest vina score was selected. Vina scores, as well as cavity size provided by the web-based server CB-dock for each binding pore are given in supplementary File Table S1.

The protein-ligand complex with a vina score of -7.7 kJ/mol was considered the most stable. Molecular docking results showed strong binding of Zapotin with *PKCε*. Visualization through ligplot^{+} indicated hydrophobic interactions between Zapotin and *PKCε* (Fig. 3a and b). Nine hydrophobic interactions were generated with Ile128, Arg282, Tyr126, Val127, Glu677, Lys663, Met521, Trp673 and Glu525 of PKCε. Among these residues, five fall in the C-terminal kinase domain and four in the N-terminal regulatory domain.

Dynamics of Zapotin binding to PKCε

To further ascertain the binding affinity of PKCε and Zapotin, a molecular dynamics simulation of 10 ns was performed that provided structural and mechanistic insight into PKCε and Zapotin interaction. RMSD and RMSF analysis revealed the stability of the structural binding of Zapotin and PKCε (Fig. 3c and d). RMSD values were below 1 A° in the 10 ns simulation, indicating that the interaction of Zapotin is within the binding pocket of PKCε. Calculations for RMSF indicated major fluctuations in residues 24–86, 195–252, and 314–378. Comparison of RMSF values with docked structure revealed that Zapotin did not interact with these residues of PKCε, and regions that had hydrophobic interactions with the drug showed comparatively fewer fluctuations. Furthermore, residues 24–86, 195–252, and 314–378 fall under the regulatory domain and hinge region of PKCε and have loop structure, which might also contribute to increased fluctuation in these regions during simulation.

The number of hydrogen bonds increased with the passage of simulation, indicating enhanced stability of Zapotin and PKCε binding over time (Fig. 3e). At the beginning of the simulation, the max hydrogen bond number was 2 and increased to 4 at 7 ns. PKCε and Zapotin binding mainly include hydrophobic interactions. The formation of a hydrophobic interaction results in the release of water molecules. Released water molecules create an aqueous pocket near the docked complexes where directional or nondirectional water molecules eventually form hydrogen bonds and contribute to atypical entropic and enthalpic penalties of hydration [70]. This presents possible reasons behind the increased rate of hydrogen bond formation over time.

Binding energies Coul-SR and LJ-SR were the main contributors to the interaction between PKCε and Zapotin. The average energy parameters obtained through MD simulation are −8.10978 KJ/mol for coul-SR and −115.328 KJ/mol for LJ-SR (Fig. 3f). LJ-SR represents repulsive energies and is dominant compared to coul-SR, which depicts attractive energy. Both short-range energy forms decreased with increased simulation time, supporting the enhanced stability of the bound PKCε-Zapotin complex with time.

Cytotoxic potential of Zapotin

The cytotoxicity potential of Zapotin was first evaluated through an MTT assay in a non-transformed Vero cell line to exclude the possibility of its toxic and non-specific influence. Zapotin treatment to Vero cells was given at concentrations ranging from 0.15μM to 0.32μM. The outcomes showed that Zapotin was non-toxic for normal cells at these concentrations (Fig. 4a). Breast cancer cells MCF-7 and MDA-MB-231 were treated with Zapotin at concentrations ranging from 0.15μM to 0.32 μM. The assay revealed that Zapotin treatment reduced the viability of the breast cancer cells and suppressed cell proliferation in a dose-dependent manner. The half maximal inhibitory concentration (IC50) determined for MCF-7 was 0.18μM and for MDA-MB-231 was 0.17μM (Fig. 4b and c). Furthermore, in both cell lines, a decrease in cancer cell growth in a dose-dependent manner was found (Fig. 4d). The growth of MCF-7 was significantly decreased at a dosage of 0.18μM, whereas MDA-MB-231 was highly sensitive to Zapotin at 0.17μM dosage.

Zapotin influence on breast cancer cell colony formation ability and migration

The effect of Zapotin on colony formation and migratory potential was also assessed in breast cancer cells. MCF-7

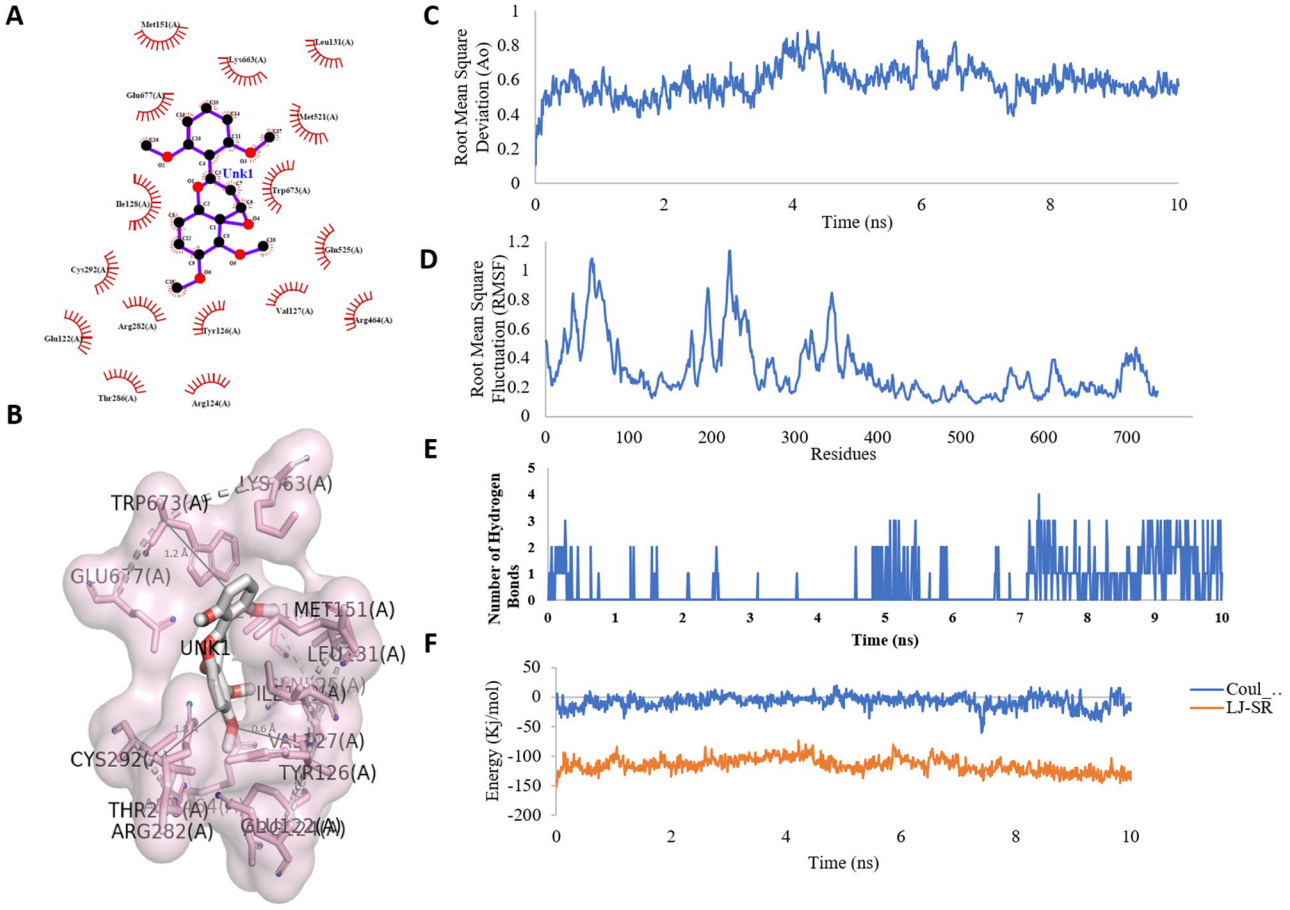

Fig. 3 Molecular interaction between Zapotin and PKCε. **A**) LigPlus^{+} two-dimensional diagram of molecular docking. Nine hydrophobic interactions are observed between PKCε and Zapotin. Hydrophobic interactions are indicated with red spikes. **B**) Three-dimensional representation of non-electrostatic interactions between PKCε and Zapotin. Oxygen atoms in ligands are depicted in red, while double-bonded oxygen in protein is shown in blue. Trajectories of Zapotin and PKCε MD simulations are calculated through **C**) Root mean square deviation (RMSD), **D**) Root mean square fluctuations (RMSF), (**E**) number of hydrogen bonds, and (**F**) energy parameters

and MDA-MB-231 cell lines were treated with Zapotin at different concentrations and the results revealed that the migratory potential of both breast cancer cell lines was remarkably reduced by Zapotin treatment (Fig. 4e). Similarly, a dose-dependent decrease in the colony-forming ability of both MCF-7 and MDA-MB-231 cells was observed. Zapotin treatment brought about a reduction in the colony size and in the total number of colonies compared to the control (Fig. 4f).

Zapotin pro-apoptotic potential in breast cancer cells

Zapotin's effect on the apoptosis of breast cancer cells was examined through flow cytometry, showing reduced cell viability and increased cell death in MCF-7 and MDA-MB-231 cells. In MCF-7 cells, Zapotin (0.18 µM) increased early apoptotic cells to 9.47% and raised late apoptotic cells to 73.56%. In MDA-MB-231 cells, early apoptotic cells increased to 2.41%, while late apoptotic cells rose to 73.02%. Total cell death was significantly higher in treated cells compared to controls (Fig. 4g).

Influence of Zapotin on PKCε expression in breast cancer cells

The effect of Zapotin treatment on the expression of PKCε at the mRNA level was evaluated in both breast cancer cell lines. The analysis revealed that the expression of PKCε was reduced significantly after 24 h of Zapotin treatment in both cell lines. In MDA-MB-231 cells, the expression of PKCε was reduced 100-Folds after treatment, whereas the expression of PKCε was down-regulated by 30-Folds in MCF-7 cells (Fig. 5a and b). Expression of PKCε was significantly more downregulated in MDA-MB-231 cells than in MCF-7 cells.

The expression of AKT, HIF-1α, SOCS3, and VEGF was also reduced after Zapotin treatment compared to untreated cells. Similar to PKCε, the expression of HIF-1α was significantly more down-regulated in MCF-7 cells than in MDA-MB-231 cells after 24 h of Zapotin treatment.

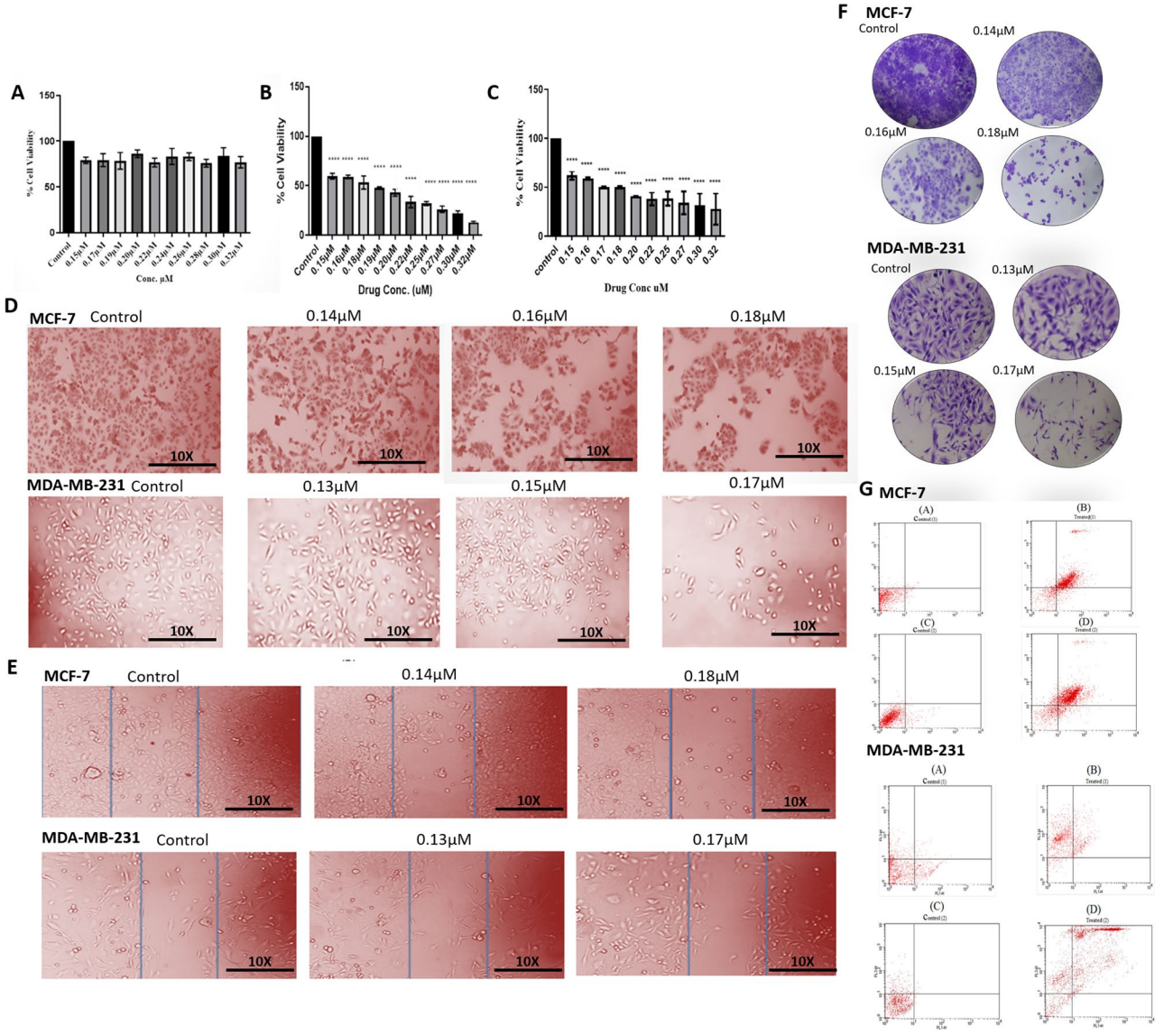

Fig. 4 Anti-cancer potential of Zapotin in breast cancer cells. Cell viability analysis of **A**) Vero, **B**) MCF-7, and **C**) MDA-MB-231 cells after 24 h treatment with Zapotin. In Vero cells, constant cell viability is observed between treated and control cells. The inhibitory effect of Zapotin is found in breast cancer cell lines. **D**) Zapotin-treated MCF-7 and MDA-MB-231 cells depicting treatment influence on cell growth. **E**) Zapotin influence on MCF-7 and MDA-MB-231 cells' migratory potential. **F**) Zapotin treatment induced colony formation ability inhibition in MCF-7 and MDA-MB-231 cells. Untreated MCF-7 and MDA-MBA-231 cells showed cell growth, migration, and colony formation, whereas treated breast cancer cells showed dose-dependent cell growth inhibition, migration suppression, and decreased colony formation. **G**) Flow cytometry analysis for Zapotin-treated breast cancer cells. *MCF-7*: **a**) Untreated MCF-7 cells displaying a high percentage of viable cells in the lower left quadrant; **b**) treated cells displaying a high percentage of late apoptotic cells in the upper right quadrant; **c**) control (untreated cells) second replicate displaying a high percentage of viable cells; **d**) treated cells displaying an increased number of late apoptotic and dead cells. *MDA-MB-231*: **a**) Control (untreated) MDA-MB-231 cells showing a high number of viable cells in the lower left quadrant; **b**) Zapotin-treated cells showing a high percentage of dead cells in the upper left quadrant; **c**) Control (untreated) second replicate with a high percentage of viable cells; **d**) Zapotin treated cells second replicate showing an increased number of late apoptotic and dead cells

Effect of Zapotin on the metabolic profile of human breast cancer cells

The MTT assay IC50s determined for MCF-7 and MDA-MB-231 were 0.18µM and 0.17µM, respectively. Therefore, these concentrations were used for studying the metabolic profile of breast cancer cells following Zapotin treatment using Gas Chromatography-Mass Spectrometry (GC-MS). The compounds obtained through GC-MS were identified using the NIST library, and their KEGG compound IDs were retrieved. Only metabolites mutually present in triplicate runs were considered for further analysis. In MCF-7, 337 metabolites were identified in untreated cells, whereas 836 metabolites were identified in Zapotin treated cells. Among these, 30 metabolites were present in both treated and untreated cells. The

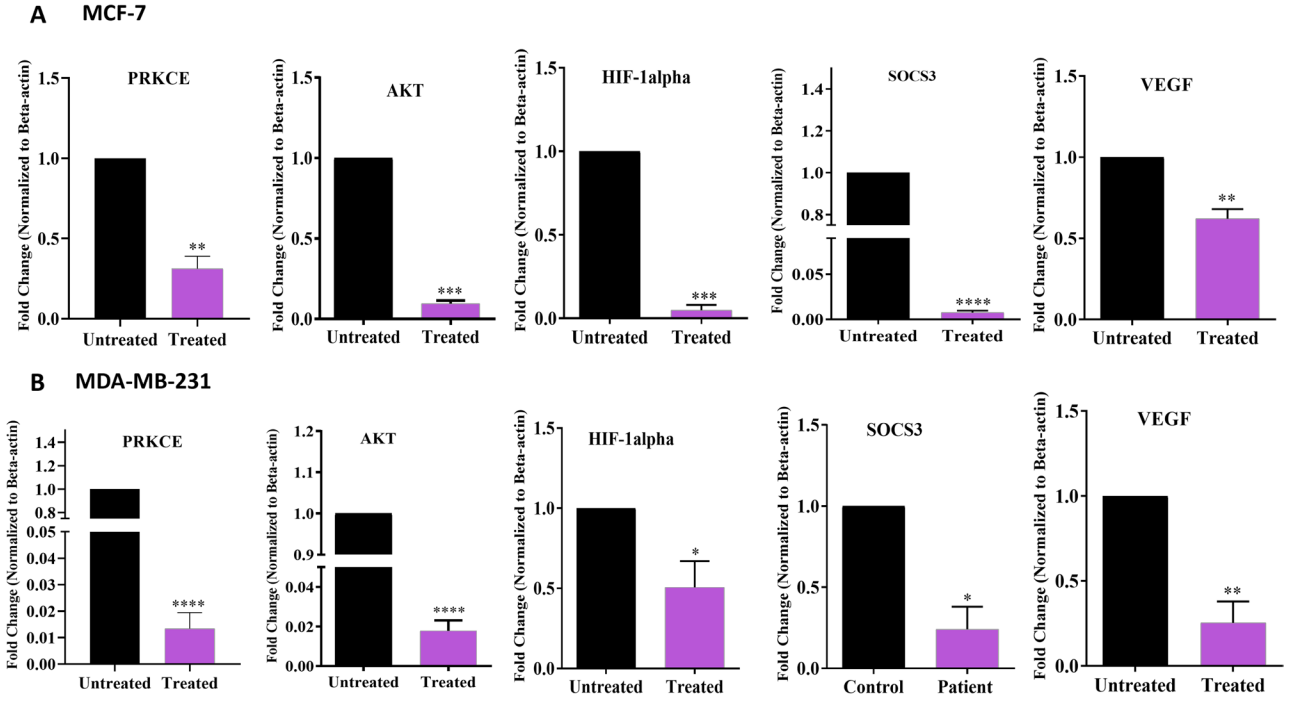

Fig. 5 Zapotin-mediated regulation of PKCε and its target expression in breast cancer. mRNA Expression of PKCε, AKT, HIF-1alpha, SOCS3, and VEGF in **A**) MCF-7 cells **B**) MDA-MB-231 cells after 24 h of Zapotin treatment. The experiments were repeated in triplicates. A P-value below 0.01 is represented as "**", below 0.005 as "***", and below 0.0001 as "****". **C**) Zapotin impact on the protein expression of PKCε, AKT, HIF-1α, and PARP in breast cancer cell lines. The protein expression of PKCε and HIF-1α reduced with an increased dosage of Zapotin in MCF-7 and MDA-MB-231 cells. The concentration of cleaved PARP after Zapotin treatment increased with increased dosage of Zapotin in MCF-7 and MDA-MB-231 cells. The protein expression of P-AKT was reduced with an increased dosage of Zapotin in MCF-7 and MDA-MB-231 cells. The immune blots presented are representative of three independent experiments with similar results. **Abbreviations**: HIF-1α (Hypoxia-inducible factor 1-alpha), PARP (poly(ADP-ribose) polymerase), SOCS3 (Suppressor of Cytokine Signaling 3), VEGF (vascular endothelial growth factor)

overlap of their chromatograms based on relative intensity indicated considerable differences in their metabolic profile (Fig. 6a and b). In MDA-MB-231, 167 metabolites were identified in Zapotin treated cells and 178 metabolites were identified in untreated cells; only four metabolites were mutually present. Chromatogram overlap between the MDA-MB-231 treatment groups indicated minor differences in metabolic profiles (Fig. 6a and b). Metabolites identified in MCF-7 cells and MDA-MB-231 after GC-MS chromatogram superimposition were then subjected to fold change analysis and ranked based on significance. The list of metabolites and their fold change are in Tables 6 and 7. In MCF-7 cells, the concentrations of 14 compounds decreased and 19 increased compared to untreated cells. Relative to MCF-7, all identified metabolites in MDA-MB-231 were down-regulated. The metabolites in both cell lines were also evaluated through principal component analysis (PCA) that revealed the distinct clustering of metabolites in Zapotin-treated as well as untreated breast cancer MDA-MB-231 and MCF-7 cells. PCA analysis depicted the variability in the metabolite profile after the treatment of Zapotin. The metabolic profile of Zapotin-treated MCF-7 and MDA-MB-231 cells is shown in Fig. 6c. The PCA analysis showed that metabolite 1,3-dimethylbenzene is present in MCF-7 and MDA-MB-231 cells. The concentration of 1,3-dimethylbenzene decreased after the treatment of Zapotin in both MCF-7 and MDA-MB-231 cells. The PCA plot for 1,3-dimethylbenzene is shown in Fig. 6d.

Gene ontology analysis of metabolic pathways

The metabolite data in both breast cancer cell lines were then processed to obtain information regarding the genes associated with these metabolites. The tool "metascape" allowed the initial identification of pathways and genes linked with metabolites. PANTHER-based gene ontology analysis was employed to determine these genes' biological, molecular, and protein functions, and the summary of the analysis outcome is provided in supplementary file figure S1. The overall analysis revealed that Zapotin modulates metabolites mostly associated with the proteins, belonging to the enzyme class "metabolite interconversion enzymes" in MDA-MB-231 and MCF-7 cells. It also regulates the function of transporter proteins, immune system proteins, and proteins associated with the translation process in MCF-7 cells. The molecular function of these proteins related to their catalytic activity, protein binding ability, transporter activity, ATP-associated

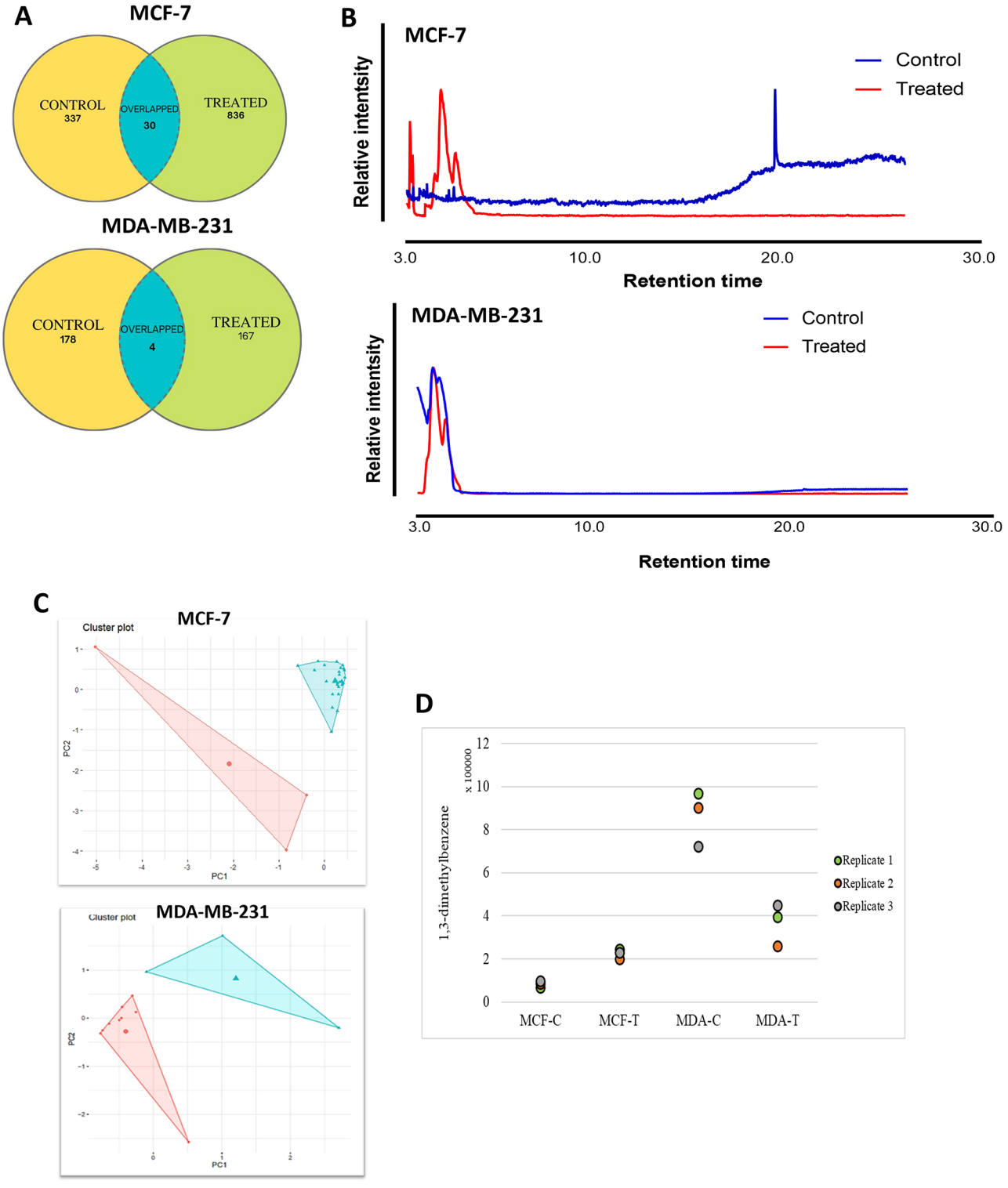

Fig. 6 Metabolic profile of Zapotin-treated and Zapotin-untreated breast cancer cell lines. **A**) Venn diagram indicating overlapping metabolites in breast cancer treated and untreated cells. **B**) Superimposed GC-MS chromatogram of treated and untreated cells. **C**) Principle component analysis (PCA) of metabolic profile of Zapotin-treated breast cancer cells. Zapotin dose 1.8µM was used for treatment. The blue plot indicates metabolites from untreated cells, and the red plot shows treated cells. (Plot created using R-Studio. **D**) PCA of metabolic 1,3-dimethylbenzene in Zapotin treated and untreated breast cancer cells. Zapotin dose 1.8µM was used for treatment. The experiment was conducted in triplicate

Table 6 GC-MS-identified metabolites in breast cancer MCF-7 cells along with their fold change

Compound name	KEGG ID	Fold Change	Significance	FDR
Cycloserine	C08057	0.068784303	2E-08	5.98E-08
Propanoic acid	C00163	0.150437285	2.37E-08	5.98E-08
Succinic acid	C00042	0.113196821	7.18E-08	1.21E-07
Propanedioic acid	C04025	17.48514635	9.77E-08	1.23E-07
Acetamide	C06244	35.29356061	3.65E-07	3.69E-07
Benzamide	C09815	0.058111531	7.28E-07	6.13E-07
Benzoic acid	C00539	0.385668265	9.09E-07	6.56E-07
Ethylbenzene	C07111	2.24653126	4.04E-06	0.000002
N6,N6-Dimethyl-adenosine	C00212	3.148195114	7.69E-06	0.000004
Cystathionine	C02291	0.299249222	2.23E-05	0.00001
D-Galactose	C00984	3.527019651	2.74E-05	0.00001
Carbamic acid	C01563	0.197520403	2.84E-05	0.00001
Benzenamine	C00292	0.431721124	3.41E-05	0.00001
Alanine	C00041	1.620756709	5.98E-05	0.00002
Imidazole	C01589	6.046602633	7.97E-05	0.00002
Diimidotricarbonic diamide	C01353	2.533978398	9.34E-05	0.00002
Piperazine	C07973	0.570111311	0.0001	0.00004
Benzene	C01407	3.736116878	0.0002	0.00006
Chloroacetic acid	C06755	1.948563193	0.0002	0.00006
Guanosine	C00387	1.929991974	0.0002	0.00006
Phosphonoacetic acid	C05682	0.11365396	0.0003	0.00007
Glutaric acid	C01601	0.512416555	0.0009	0.0002
Acetic acid	C00033	2.963418119	0.003	0.0007
3-(Ethyl-hydrazono)-butan-2-one	C02845	1.295240184	0.003	0.0007
octyl phthalate	C14227	0.016227183	0.003	0.0007
Piperidine	C01746	1.111316148	0.01	0.002
Phenol	C15584	13.28257524	0.03	0.005
Glycine	C00037	0.677608712	0.13	0.02
Cyclohexane	C11249	1.04981557	0.26	0.04
Phosphinic acid	C05339	0.965450982	0.27	0.04

Table 7 GC-MS-identified metabolites in breast cancer MDA-MB-231 cells along with their fold change

Compound name	KEGG ID	Fold Change	Significance	FDR
Benzeneacetaldehyde	C00601	0.143773723	0.001	0.00303
Octane	C01387	0.190148064	0.04	0.06015
Benzene	C01407	0.039160252	0.26	0.20391
Carbamic acid	C01563	0.847387447	0.059	0.06015

activity, and translation regulation properties were indicated by GO-annotation analysis. Overall, the analysis indicated that Zapotin targets metabolic processes as well as other integral processes that might be involved in promoting therapeutic resistance in breast cancer.

Metabolic pathways influenced by Zapotin treatment in MCF-7 cells

Enrichment analysis to determine Zapotin-influenced pathways in MCF-7 cells was performed. Based on enrichment ratio, significance value, and fold change, the results showed that Zapotin targets pathways associated with amino acid metabolism (Supplementary file figure S1). MSEA analysis indicated that Alanine, methionine, glutamate, glutathione, serine, glycine, and selenoamino acid metabolism was significantly influenced by Zapotin treatment (Fig. 7a). IPA pathway analysis revealed that the methionine degradation pathway was also active in Zapotin-treated cells (Fig. 7b). Other affected pathways corresponded to macromolecule catabolism as well as anabolism, such as purine metabolism, urea metabolism, fatty acid biosynthesis, and vitamin K metabolism. MSEA further indicated modulation of cell energy pathways and the metabolic alterations in breast MCF-7 cells.

Metabolites identified through the above enrichment analyses were subjected to network analysis to identify canonical pathways and networks through IPA. The 30 identified metabolites were fed into the software and core analysis highlighted the significant contribution of the HIF-1 pathway targeted by Zapotin treatment. Network analysis also indicated the involvement of metabolic proteins in inducing hypoxia. Proteins and metabolites associated with glycolysis, pentose phosphate pathway (PPP), and TCA cycle role also dominated. These pathways contribute to metabolic rewiring in several cancers that, by altering the energy consumption of the cell, also contribute to chemotherapy resistance. PKCε, meantime, is shown to directly activate 6-Phosphofructo-2-Kinase (PFKFB4), an integral enzyme in glycolysis. The analysis also indicated the contribution of the insulin signaling pathway. The network generated for Zapotin-treated MCF-7 cells is illustrated in Fig. 7c. Multiple central nodes were generated in response to the protein-protein network, including HSF1, EP300, and DPH5.

Metabolic pathways influenced by Zapotin treatment in MDA-MB-231 cells

The results of our enrichment analysis showed that Zapotin regulates the metabolism of amino acids, as well as the synthesis of biological precursors involved in cell metabolism. In breast MDA-MB-231 cells, substantial impacts on cell energy pathways such as the TCA cycle and pentose phosphate pathway were also observed. According to the study outcomes, Zapotin seems to play a part in regulating the metabolic pathways in MDA-MB-231 cells. IPA analysis indicated Zapotin's influence on the modulation of phenylalanine catabolism (Fig. 8a and b).

IPA-based network evaluation furthered the insight related to the phenylalanine metabolism interaction

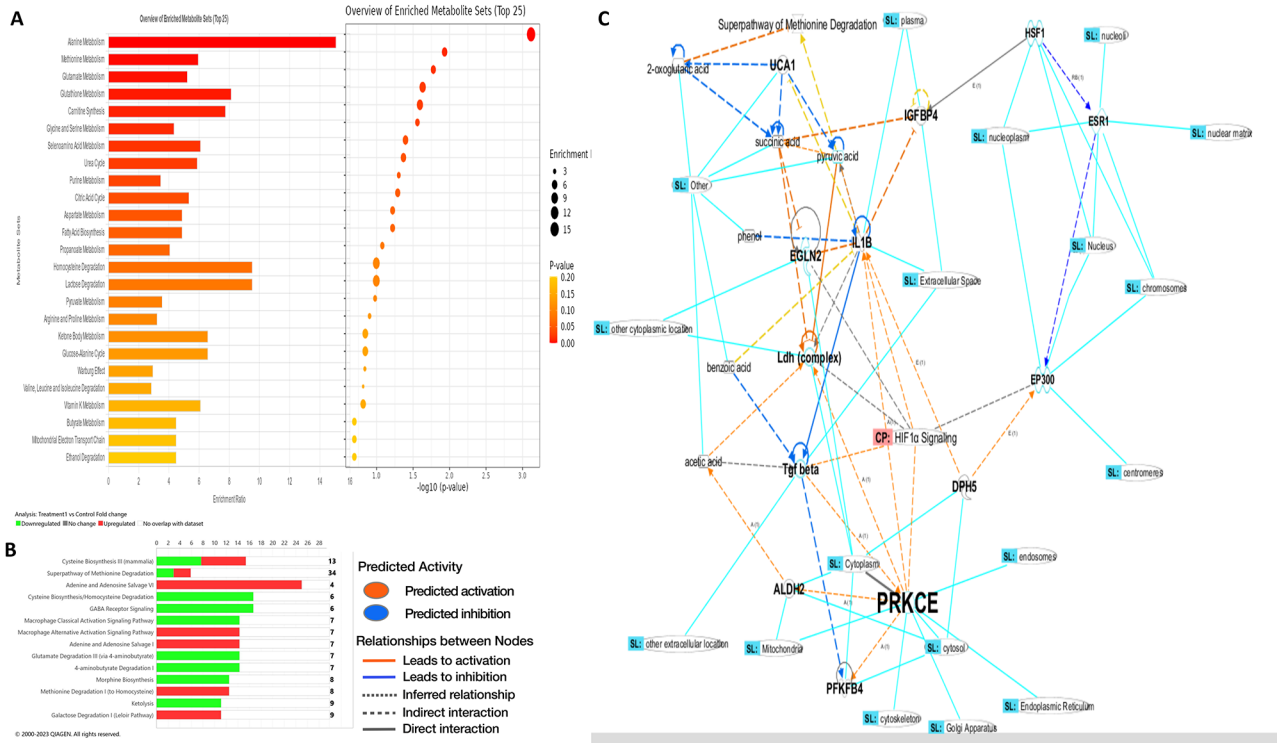

Fig. 7 Metabolite Set Enrichment Analysis **(**MSEA) and pathway analysis of the identified metabolites in MCF-7 cells. **A**) Enrichment analysis as per **a**) enrichment ratio. **b**) P-value Red indicates high significance, whereas yellow represents low significance. The size of the circle indicates the enrichment ratio. (Graphs were generated through MetaboAnalyst [94]). **B**) Number of metabolites participating in different pathways in MCF-7 cells. Most genes participated in the methionine degradation pathway. Fisher's exact test p-value determined bar length. **C**) Ingenuity Pathway Analysis (IPA) of metabolites associated with cellular proteins and associated pathways in Zapotin-treated MCF-7 cells. Orange lines indicate the activation of predicted relations. Blue lines indicate the inhibition of predicted relations. The cyan color indicates the potential cellular localization of the proteins. PKCε-mediated cellular alterations may be associated with metabolic rewiring in breast cancer cells

with malignant breast cell growth. The phenylalanine metabolism produces phenylacetaldehyde, a precursor for several metabolites of the TCA cycle. Phenylacetaldehyde may lead to the production of fumaric acid and acetyl-CoA, which are the main pathway drivers of the TCA cycle. PKCε also contributes to metabolic rewiring by activating the PPP pathway. It also induces the production of succinate (TCA cycle molecule) via pyruvate (Fig. 8c and Supplementary Figure S2).

Discussion

Research has identified the contribution of numerous molecular components in breast cancer development. Several biomarkers such as HER2, CEA, TPA, and the ABC transporter protein family, has specifically been [71]. Investigations further revealed the role of over-expressed PKCε in cancer cells in promoting these proteins' expression and surface availability through modulating PI3K/Akt signaling and MAPK/ERK pathway [17, 72]. Targeting PKCε through naturally-occurring compounds has shown a reversal of cancer hallmarks and induction of apoptosis [17, 73]. Zapotin, an isoflavonoid, has been reported to target the expression of PKCε in HeLa cells, which reduces the migratory potential of cancer cells and induces apoptosis [29, 74]. However, the influence of Zapotin on the expression and activity of PKCε in breast cancer is not reported. The current study aimed to analyze the binding efficacy of PKCε with Zapotin through in silico analysis as well as the effects of Zapotin-induced PKCε inhibition on breast cancer cell viability, growth, and invasiveness.

In silico pharmacokinetic analysis of Zapotin indicated its high intestinal absorption and oral bioavailability, suggesting oral ingestion as its possible route of administration. Its skin permeation value was also in the favorable range. Skin permeability (LogK) co-efficient value mainly depends on the membrane of the skin. Skin membrane with epidermis and dermis requires more hydrophilicity for penetration while skin membrane consisting of stratum corneum governs more lipophilic properties in drug for absorption [75]. Zapotin has been estimated to have lipophilic and hydrophilic properties that indicate skin as it's another possible route of administration.

Drugs or xenobiotics are metabolized by the action of the CYP450 enzyme system in hepatic cells. Zapotin was predicted to act as the inhibitor for some CYP450

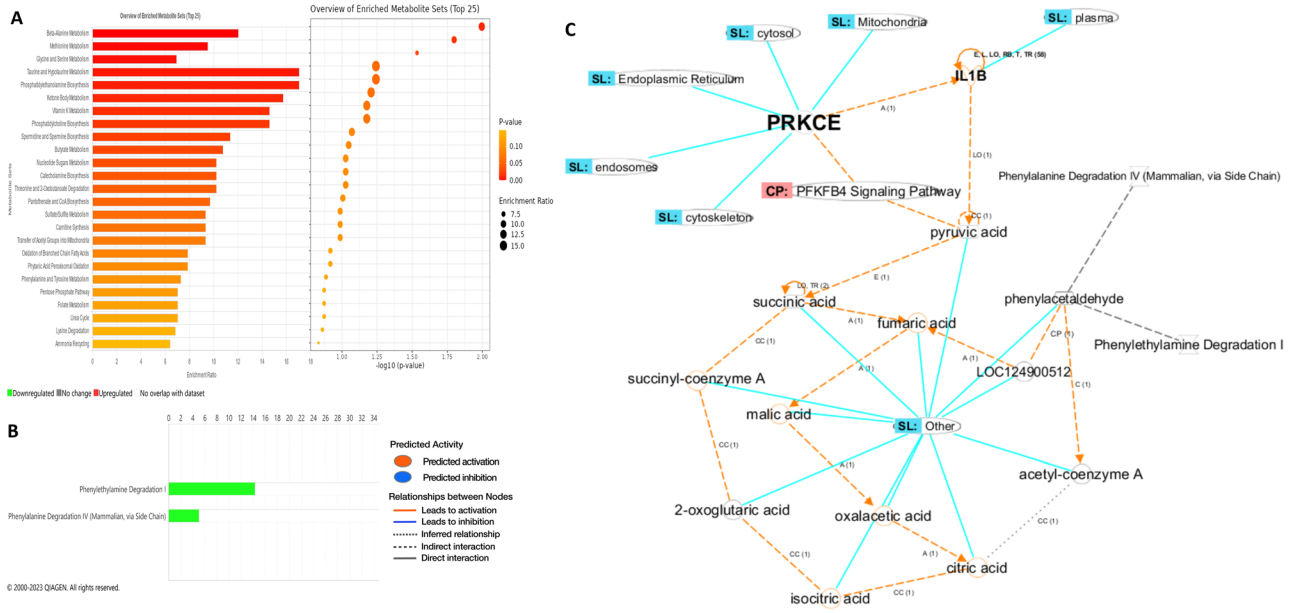

Fig. 8 Metabolite Set Enrichment Analysis (MSEA**)** and pathway analysis of the identified metabolites in MDA-MB-231 cells. **A**) Enrichment analysis as per **a**) enrichment ratio. **b**) P-value Red indicates high significance, whereas yellow represents low significance. The size of the circle indicates the enrichment ratio. (Graphs were generated through MetaboAnalyst [94]). **B**) Number of metabolites participating in different pathways in MDA-MB-231 cells. Most genes participated in the methionine degradation pathway. Fisher's exact test p-value determined bar length. **C**) Ingenuity Pathway Analysis (IPA) of metabolites associated with cellular proteins and associated pathways in Zapotin-treated MDA-MB-231 cells. Orange lines indicate the activation of predicted relations. Blue lines indicate the inhibition of predicted relations. The cyan color indicates the potential cellular localization of the proteins. PKCε-mediated cellular alterations may be associated with metabolic rewiring in breast cancer cells

enzymes that might influence the proper metabolism of co-administered compounds, leading to drug accumulation and cytotoxicity [68, 69]. Further, the efficacy of CYP450 enzymes in metabolizing particular drugs strongly depends on genetic polymorphism [76]. Therefore, studies delineating the influence of polymorphism in CYP450 enzymes on Zapotin metabolism will be advantageous in understanding its pharmacokinetics. In silico pharmacokinetics analysis in the current study further estimated the safety of its ingestion without any possible adverse toxic effect. However, at higher doses, Zapotin might bring about liver toxicity and arrhythmia.

In silico pharmacokinetics analysis of Zapotin revealed its possible interaction and resultant inhibition of kinases. PKCε is a serine/threonine kinase that has been demonstrated to play a chief role in numerous cancers, including breast cancer. Molecular docking and MD simulation analysis showed strong and stable interaction of Zapotin with PKCε. The major bonding interaction estimated between PKCε and Zapotin was non-electrostatic hydrophobic interaction. Formation of hydrophobic interactions between ligand's lipophilic groups and protein's non-polar side chains results in gaining free binding energy. It changes the thermodynamics of ligand binding with protein, leading to enhanced binding affinity [77]. A study demonstrated that integrating functional groups in the ligand that favor hydrophobic interactions enhances drug-protein interaction stability and binding affinity [78]. MD simulation analysis revealed that the interaction of PKCε and Zapotin stabilizes over time. Molecular docking and MD simulation outcomes further revealed that Zapotin makes hydrophobic interactions at the kinase domain of PKCε. The N-terminal kinase domain of PKCε has two essential regions, ATP-binding site and active site, that play a key role in the phosphorylation of its substrate [79, 80]. Zapotin binding with these regions impairs its phosphorylation capacity. Further, Zapotin interacts with the regulatory domain and retards PKC activation through DAG by binding the C1A-C1B domain [81, 82]. Thus, in silico approaches have revealed that Zapotin has great potential in inhibiting PKCε activity and estimated administration safety.

Investigation of Zapotin's influence on the growth, proliferation, and invasiveness of breast cancer MCF-7 and MDA-MB-231 cells showed the dose-dependent inhibition of cells growth and migratory potential. Moreover, Zapotin induced programmed cell death of breast cancer cells in a concentration-dependent manner. Expression analysis revealed that PKCε expression was down-regulated by Zapotin treatment in MCF7 and MDA-MB-231 cells. Zapotin treatment also down-regulated HIF-1α and Akt expression at transcriptional as well as translational levels. Previously, Zapotin-mediated inhibition of PKCε was studied in HeLa cell lines, demonstrating

dose-dependent inhibition of cell migration and increased apoptotic cell fraction [74]. Zapotin treatment in HeLa cells also modulated the autophagy pathway by decreasing the protein concentration of microtubule-associated protein 1 light chain 3 and hindering autophagosome formation. Autophagy inhibition leads to the induction of cell death in HeLa cells [29]. PKCε-mediated autophagy has been involved in promoting the survival of glioma cells by enhancing tolerance to stress and the emergence of resistance against anti-cancer cells [83]. PKCε interacts with MDR1 leading to gemcitabine resistance and the development of colony-forming potential in cancer cells [84, 85].

Cancer cells alter their metabolic signaling to promote cancer survival, leading to the development of mechanisms within cancer cells that also facilitate resistance to cancer treatment [86–88]. Therefore, in the present study, metabolic profiling and network analyses of breast cancer cell lines MCF7 and MDA-MB-271 were performed to analyze the impact of Zapotin treatment. The gene ontology analysis depicted Zapotin influences metabolic pathways and metabolite interconversion enzymes in MCF-7 and MDA-MB-231 cell lines. In MCF-7, the network layout depicted the contribution of HIF1 signaling in metabolic rewiring. HIF1 promotes glucose metabolism through the aerobic pathway [87]. HIF1 and PKCε role in the metabolic alteration of breast cancer cells was also observed in the present study. PFKBP3 is a glycolytic pathway enzyme, and PKCε was found to activate PFKBP3 in breast cancer directly. Overexpression of PKCε meantime may increase the activation rate of PFKBP3, resulting in enhanced pyruvate production. The enhanced glycolysis rate supports the metabolic alteration in cancer cells, allowing them to accumulate bioprecursors for cancer cell proliferation and division [89]. As hypoxia is a state of lower oxygen, these metabolic alterations also allows cancer cells to produce energy without oxygen by converting pyruvate into lactate [90]. Studies also indicated that regulation od ROS, glycolysis, and ERS pathways also promote sensitization in cancer cells [91–93]. The present study depicted the key involvement of PKCε in promoting metabolic alteration in breast cancer. These metabolic alterations might also contribute to Warburg effect that is a key event in therapy resistance in cancers including breast cancer. Our study clearly indicated the role of PRKCE in modulating glycolytic pathway. Glycolytic pathway is among the initial events in Warburg effect in which cancer cells start producing lactate as glycolysis end-product that enhances oxidative stress and further modulate other metabolic pathways to support cancer growth [90].

The comparison of Zapotin's influence on MCF-7 vs. MDA-MB-231 indicate that Zapotin influenced cell proliferation, migratory potential, hypoxia markers' gene expression, and metabolom of both cell lines. However, MDA-MB-231 appeared to be more sensitive to Zapotin's treatment. Firstly, its IC50 was lower (0.17μM) than MCF-7 (0.18μM). The expression of molecular markers PRKCE, AKT, and VEGF was suppressed several folds (0.01 ($p < 0.001$), 0.015 ($p < 0.001$), and 0.2 ($p < 0.05$)) in MDA-MB-231 in comparison to MCF-7. Flow cytometry results also indicated more pronounced number of cells in the late apoptotic and dead stage in MDA-MB-231 cell.

Conclusion

Zapotin has the potential to bind and inhibit the activity of PKCε and hence, curb breast cancer carcinogenicity. Metabolic profile analysis further revealed that PKCε promotes hypoxia in breast cancer that may contribute to metabolic rewiring. Lastly, in silico evaluation of Zapotin estimated its safe clinical implementation, good bioavailability, and low toxicity. Considering Zapotin's potential in targeting metabolic pathways of breast cancer cells, further studies are warranted to understand its role in curbing cancer resistance. To determine its safety, studies in animal models are required. As Zapotin was found to target PKCε in breast cancer cell lines; its further novel molecular targets should be studied. The study outcomes provide essential insight into the mechanism of PKCε mediated cell signaling and suggested PKCε as a potent maker to be translated and explored at animal as well as human level. Future studies delineating its role and safety profile in rodent or dogs animal models will be a step forward in translating this study at clinical level.

Limitations

The study outcomes offer information about the anticancer properties of Zapotin against breast cancer cells MCF-7 and MDA-MB-231. However, the study is limited to in vitro model and the lack of in vivo validation may limit its translations to clinical relevance. Likewise, metabolomic analysis provided valuable insight on its mechanism of actions, the manual infiltration method along with limited sample size may have vailed further biologically relevant metabolites. Future investigations involving animal studies and broader metabolite profiling may expand upon these results.

Supplementary Information

The online version contains supplementary material available at https://doi.org/10.1186/s12885-025-14202-z.

Supplementary Material 1

Acknowledgements

The authors extend their appreciation to the Researchers Supporting project number (RSPD2025R729), King Saud University, Riyadh Saudi Arabia for funding this project.

Author contributions
MS, YB, KK, MA, NMA, SR, AH, and TA designed the study, conceived the study and analyzed the results. KK, NMA, SR, TA, FMH, DK and AH conceived an initial part of the study, performed the experiment, and helped in compiling the results. MS and YB experimented. KK, MA, SR, FMH, SR, and TA helped in writing the results. SR, TA, DK, and FMH wrote the paper with input from all other authors MS, SR, YB, KK, TA, NMA, JHT, AH and FMH made a substantial contribution in the interpretation of data and revising the manuscript for intellectual content. NMA performed bioinformatics. All authors read and approved the final manuscript.

Funding
The authors extend their appreciation to the Researchers Supporting project number (RSPD2025R729), King Saud University, Riyadh Saudi Arabia for funding this project. The funding body has no role in designing the study.

Data availability
All data generated or analyzed during this study are included in this article.

Declarations

Ethics approval and consent to participate
The experimental protocol for the use of human blood samples was approved (Ref: No: IRB No. 04-2019-03/06) by the ethical committee of Combined Military Hospital and ASAB, NUST. Informed consent was obtained from all subjects and/or their legal guardian(s).The study was done in accordance with Declaration of Helsinki.

Consent for publication
Not applicable.

Competing interests
The authors declare no competing interests.

Received: 28 January 2025 / Accepted: 22 April 2025
Published online: 28 April 2025

References

1. Siegel RL, Giaquinto AN, Jemal A. *Cancer statistics*, 2024. CA: a cancer journal for clinicians, 2024. 74(1): pp. 12–49.
2. Siegel RL, et al. Cancer statistics, 2021. Cancer J Clin. 2021;71(1):7–33.
3. Bray F, et al. Global cancer statistics 2018: GLOBOCAN estimates of incidence and mortality worldwide for 36 cancers in 185 countries. Cancer J Clin. 2018;68(6):394–424.
4. Huang J, et al. Global incidence and mortality of breast cancer: a trend analysis. Aging. 2021;13(4):5748.
5. Tang Y, et al. Classification, treatment strategy, and associated drug resistance in breast cancer. Clin Breast Cancer. 2016;16(5):335–43.
6. Longley D, Johnston P. Molecular mechanisms of drug resistance. J Pathology: J Pathological Soc Great Br Irel. 2005;205(2):275–92.
7. Ahmad A. Breast Cancer metastasis and drug resistance: challenges and progress. Volume 1152. Springer; 2019.
8. Liu J, et al. Exosomes from tamoxifen-resistant breast cancer cells transmit drug resistance partly by delivering miR-9-5p. Cancer Cell Int. 2021;21(1):1–15.
9. Kim D-S, et al. Reversal of drug resistance in breast cancer cells by transglutaminase 2 Inhibition and nuclear factor-κB inactivation. Cancer Res. 2006;66(22):10936–43.
10. Dong C, et al. Activation of PI3K/AKT/mTOR pathway causes drug resistance in breast Cancer. Front Pharmacol. 2021;12:143.
11. Wang J, et al. Salvianolic acid B suppresses EMT and apoptosis to lessen drug resistance through AKT/mTOR in gastric cancer cells. Cytotechnology. 2021;73(1):49–61.
12. Caino MC, et al. Non-small cell lung carcinoma cell motility, Rac activation and metastatic dissemination are mediated by protein kinase C epsilon. PLoS ONE. 2012;7(2):e31714.
13. Basu A. Regulation of autophagy by protein kinase C-ε in breast Cancer cells. Int J Mol Sci. 2020;21(12):4247.
14. Peng Y, et al. Andrographolide inhibits breast cancer through suppressing COX-2 expression and angiogenesis via inactivation of p300 signaling and VEGF pathway. J Experimental Clin Cancer Res. 2018;37(1):1–14.
15. Hu H, et al. Elevated COX-2 expression promotes angiogenesis through EGFR/p38-MAPK/Sp1-dependent signalling in pancreatic cancer. Sci Rep. 2017;7(1):1–10.
16. Fouad YA, Aanei C. Revisiting the hallmarks of cancer. Am J cancer Res. 2017;7(5):1016.
17. Huang B, et al. PKCε inhibits isolation and stemness of side population cells via the suppression of ABCB1 transporter and PI3K/Akt, MAPK/ERK signaling in renal cell carcinoma cell line 769P. Cancer Lett. 2016;376(1):148–54.
18. Martin-Orozco E, et al. WNT signaling in tumors: the way to evade drugs and immunity. Front Immunol. 2019;10:2854.
19. Greco S, Storelli C, Marsigliante S. Protein kinase C (PKC)-δ/-ε mediate the PKC/Akt-dependent phosphorylation of extracellular signal-regulated kinases 1 and 2 in MCF-7 cells stimulated by Bradykinin. J Endocrinol. 2006;188(1):79–89.
20. Wu D, et al. PKC-β1 mediates glucose-induced Akt activation and TGF-β1 upregulation in mesangial cells. J Am Soc Nephrol. 2009;20(3):554–66.
21. Schmitz-Peiffer C. Deconstructing the role of PKC epsilon in glucose homeostasis. Trends Endocrinol Metabolism. 2020;31(5):344–56.
22. Gassaway BM, et al. PKCε contributes to lipid-induced insulin resistance through cross talk with p70S6K and through previously unknown regulators of insulin signaling. Proc Natl Acad Sci. 2018;115(38):E8996–9005.
23. McCarthy J, et al. PKCε promotes cardiac mitochondrial and metabolic adaptation to chronic hypobaric hypoxia by GSK3β Inhibition. J Cell Physiol. 2011;226(9):2457–68.
24. Rathore R, et al. Mitochondrial ROS-PKCε signaling axis is uniquely involved in hypoxic increase in [Ca2+] i in pulmonary artery smooth muscle cells. Biochem Biophys Res Commun. 2006;351(3):784–90.
25. Garg R et al. *Requirement for PKC Epsilon in Kras-Driven Lung Tumorigenesis.* bioRxiv, 2020.
26. Ranieri D, et al. Role of PKCε in the epithelial-mesenchymal transition induced by FGFR2 isoform switch. Cell Communication Signal. 2020;18(1):1–13.
27. Garg R, et al. COX-2 mediates pro-tumorigenic effects of PKCε in prostate cancer. Oncogene. 2018;37(34):4735–49.
28. Xu W, et al. Crosstalk of protein kinase C ε with Smad2/3 promotes tumor cell proliferation in prostate cancer cells by enhancing aerobic Glycolysis. Cell Mol Life Sci. 2018;75(24):4583–98.
29. Toton E, et al. Zapotin (5, 6, 2′, 6′-tetramethoxyflavone) modulates the crosstalk between autophagy and apoptosis pathways in cancer cells with overexpressed constitutively active PKCε. Nutr Cancer. 2016;68(2):290–304.
30. Kanade GG, et al. Zapotin mediates its action by inducing p53 in wild-type p53 positive human lung cancer cells. AACR; 2010.
31. Strawa JW, Jakimiuk K, Tomczyk M. Zapotin, a polymethoxyflavone, with potential therapeutic attributes. Int J Mol Sci. 2021;22(24):13227.
32. Maiti A, et al. Synthesis and cancer chemopreventive activity of Zapotin, a natural product from Casimiroa edulis. J Med Chem. 2007;50(2):350–5.
33. Cuendet M, et al. Zapotin prevents mouse skin tumorigenesis during the stages of initiation and promotion. Anticancer Res. 2008;28(6A):3705–9.
34. Murillo G, et al. Zapotin, a phytochemical present in a Mexican fruit, prevents colon carcinogenesis. Nutr Cancer. 2007;57(1):28–37.
35. Khan K, et al. Influence of PRKCE non-synonymous variants on protein dynamics and functionality. Human Molecular Genetics; 2022.
36. Yang J, Zhang Y. I-TASSER server: new development for protein structure and function predictions. Nucleic Acids Res. 2015;43(W1):W174–81.
37. Dym O, Eisenberg D, Yeates T. ERRAT 2012.
38. Almagro Armenteros JJ, et al. DeepLoc: prediction of protein subcellular localization using deep learning. Bioinformatics. 2017;33(21):3387–95.
39. Krogh A, et al. Predicting transmembrane protein topology with a hidden Markov model: application to complete genomes. J Mol Biol. 2001;305(3):567–80.
40. Almagro Armenteros JJ, et al. SignalP 5.0 improves signal peptide predictions using deep neural networks. Nat Biotechnol. 2019;37(4):420–3.
41. Nielsen H, et al. Predicting eukaryotic protein secretion without signals. Biochim Et Biophys Acta (BBA)-Proteins Proteom. 2019;1867(12):p140174.
42. Emanuelsson O, et al. Locating proteins in the cell using TargetP, signalp and related tools. Nat Protoc. 2007;2(4):953–71.
43. Wolber G, Langer T. LigandScout: 3-D pharmacophores derived from protein-bound ligands and their use as virtual screening filters. J Chem Inf Model. 2005;45(1):160–9.

44. Cheminformatics M. *Nova ulica, SK-900 26 Slovensky Grob, Slovak Republic*. 2018.
45. Yang H, et al. AdmetSAR 2.0: web-service for prediction and optimization of chemical ADMET properties. Bioinformatics. 2019;35(6):1067–9.
46. Taj T, et al. One-pot synthesis of pyrazoline derivatised carbazoles as antitubercular, anticancer agents, their DNA cleavage and antioxidant activities. Eur J Med Chem. 2011;46(9):4366–73.
47. Tseng YJ et al. *Steps Toward a Virtual Rat: Predictive Absorption, Distribution, Metabolism, and Toxicity Models*. in *Frontiers in Molecular Design and Chemical Information Science-Herman Skolnik Award Symposium 2015: Jürgen Bajorath*. 2016. ACS Publications.
48. Ivanov SM, et al. ADVERPred–web service for prediction of adverse effects of drugs. J Chem Inf Model. 2018;58(1):8–11.
49. Daina A, Michielin O, Zoete V. SwissADME: a free web tool to evaluate pharmacokinetics, drug-likeness and medicinal chemistry friendliness of small molecules. Sci Rep. 2017;7(1):1–13.
50. Liu Y, et al. CB-Dock: a web server for cavity detection-guided protein–ligand blind Docking. Acta Pharmacol Sin. 2020;41(1):138–44.
51. Laskowski RA, Swindells MB. LigPlot+: multiple ligand–protein interaction diagrams for drug discovery. ACS; 2011.
52. Van Der Spoel D, et al. GROMACS: fast, flexible, and free. J Comput Chem. 2005;26(16):1701–18.
53. Rio DC, et al. Purification of RNA using trizol (TRI reagent). Cold Spring Harbor Protoc. 2010;20106:pdbprot5439.
54. Adams G. A beginner's guide to RT-PCR, qPCR and RT-qPCR. Biochemist. 2020;42(3):48–53.
55. Livak KJ, Schmittgen TD. Analysis of relative gene expression data using real-time quantitative PCR and the 2– ΔΔCT method. Methods. 2001;25(4):402–8.
56. Semreen MH, et al. Comparative metabolomics of MCF-7 breast cancer cells using different extraction solvents assessed by mass spectroscopy. Sci Rep. 2019;9(1):1–9.
57. Kanehisa M, et al. KEGG: new perspectives on genomes, pathways, diseases and drugs. Nucleic Acids Res. 2017;45(D1):D353–61.
58. Xu J, et al. An optimized analytical method for cellular targeted quantification of primary metabolites in Tricarboxylic acid cycle and Glycolysis using gas chromatography-tandem mass spectrometry and its application in three kinds of hepatic cell lines. J Pharm Biomed Anal. 2019;171:171–9.
59. Benjamini Y, et al. Controlling the false discovery rate in behavior genetics research. Behav Brain Res. 2001;125(1–2):279–84.
60. Ibáñez C, et al. GC-MS based metabolomics of colon cancer cells using different extraction solvents. Anal Chim Acta. 2017;986:48–56.
61. Smoot ME, et al. Cytoscape 2.8: new features for data integration and network visualization. Bioinformatics. 2011;27(3):431–2.
62. Mi H, et al. PANTHER version 14: more genomes, a new PANTHER GO-slim and improvements in enrichment analysis tools. Nucleic Acids Res. 2019;47(D1):D419–26.
63. Consortium GO. The gene ontology (GO) database and informatics resource. Nucleic Acids Res. 2004;32(suppl1):D258–61.
64. Krämer A, et al. Causal analysis approaches in ingenuity pathway analysis. Bioinformatics. 2014;30(4):523–30.
65. Lipinski CA, et al. Experimental and computational approaches to estimate solubility and permeability in drug discovery and development settings. Adv Drug Deliv Rev. 1997;23(1–3):3–25.
66. Veber DF, et al. Molecular properties that influence the oral bioavailability of drug candidates. J Med Chem. 2002;45(12):2615–23.
67. Ertl P, Schuffenhauer A. Estimation of synthetic accessibility score of drug-like molecules based on molecular complexity and fragment contributions. J Cheminform. 2009;1(1):1–11.
68. Lynch T, Price AL. The effect of cytochrome P450 metabolism on drug response, interactions, and adverse effects. Am Family Phys. 2007;76(3):391–6.
69. Ghosh D, et al. Novel aromatase inhibitors by structure-guided design. J Med Chem. 2012;55(19):8464–76.
70. Young T, et al. Motifs for molecular recognition exploiting hydrophobic enclosure in protein–ligand binding. Proc Natl Acad Sci. 2007;104(3):808–13.
71. Li J, et al. Non-invasive biomarkers for early detection of breast cancer. Cancers. 2020;12(10):2767.
72. Scerri J, et al. PKC-mediated phosphorylation and activation of the MEK/ERK pathway as a mechanism of acquired trastuzumab resistance in HER2-positive breast cancer. Front Endocrinol. 2022;13:1010092.
73. Hafeez BB, et al. Genetic ablation of PKC epsilon inhibits prostate cancer development and metastasis in Transgenic mouse model of prostate adenocarcinoma. Cancer Res. 2011;71(6):2318–27.
74. Toton E, et al. The tetramethoxyflavone Zapotin selectively activates protein kinase C epsilon, leading to its down-modulation accompanied by Bcl-2, c-Jun and c-Fos decrease. Eur J Pharmacol. 2012;682(1–3):21–8.
75. N'Da DD. Prodrug strategies for enhancing the percutaneous absorption of drugs. Molecules. 2014;19(12):20780–807.
76. Weckwerth GM, et al. CYP450 polymorphisms and clinical pharmacogenetics of ibuprofen after lower third molar extraction. Eur J Clin Pharmacol. 2021;77(5):697–707.
77. Snyder P P.W., et al. Mechanism of the hydrophobic effect in the biomolecular recognition of arylsulfonamides by carbonic anhydrase. Proc Natl Acad Sci. 2011;108(44):17889–94.
78. Patil R, et al. Optimized hydrophobic interactions and hydrogen bonding at the target-ligand interface leads the pathways of drug-designing. PLoS ONE. 2010;5(8):e12029.
79. Akita Y. Protein kinase C-ε (PKC-ε): its unique structure and function. J Biochem. 2002;132(6):847–52.
80. Schaap D, Parker PJ. Expression, purification, and characterization of protein kinase C-epsilon. J Biol Chem. 1990;265(13):7301–7.
81. Pany S, Das J. Alcohol binding in the C1 (C1A + C1B) domain of protein kinase C epsilon. Biochim Et Biophys Acta (BBA)-General Subj. 2015;1850(11):2368–76.
82. Blumberg P, et al. Wealth of opportunity-the C1 domain as a target for drug development. Curr Drug Targets. 2008;9(8):641–52.
83. Toton E, et al. Impact of PKCε downregulation on autophagy in glioblastoma cells. BMC Cancer. 2018;18(1):1–17.
84. Zhang G-F et al. Overexpression of microRNA-205-5p exerts suppressive effects on stem cell drug resistance in gallbladder cancer by down-regulating PRKCE. Biosci Rep, 2020. 40(9).
85. Wang H, et al. miR-218-5p restores sensitivity to gemcitabine through PRKCE/MDR1 axis in gallbladder cancer. Cell Death Dis. 2017;8(5):e2770–2770.
86. Epple LM, et al. Induction of the unfolded protein response drives enhanced metabolism and chemoresistance in glioma cells. PLoS ONE. 2013;8(8):e73267.
87. Belisario DC, et al. Hypoxia dictates metabolic rewiring of tumors: implications for chemoresistance. Cells. 2020;9(12):2598.
88. Huang Y, et al. Energy blocker Lonidamine reverses nimustine resistance in human glioblastoma cells through energy Blockade, redox homeostasis disruption, and O 6-Methylguanine-DNA methyltransferase downregulation: in vitro and in vivo validation. Volume 7. ACS Pharmacology & Translational Science; 2024. pp. 1518–32. 5.
89. Schwartz L, Supuran CT, Alfarouk KO. The Warburg effect and the hallmarks of cancer. Anti-Cancer Agents Med Chem (Formerly Curr Med Chemistry-Anti-Cancer Agents). 2017;17(2):164–70.
90. Courtnay R, et al. Cancer metabolism and the Warburg effect: the role of HIF-1 and PI3K. Mol Biol Rep. 2015;42:p841–851.
91. Sun X, et al. 2-Deoxy-D-glucose increases the sensitivity of glioblastoma cells to BCNU through the regulation of glycolysis, ROS and ERS pathways: in vitro and in vivo validation. Biochem Pharmacol. 2022;199:115029.
92. Sun X, et al. 3-Bromopyruvate regulates the status of Glycolysis and BCNU sensitivity in human hepatocellular carcinoma cells. Biochem Pharmacol. 2020;177:113988.
93. Sun X, et al. Glycolytic Inhibition by 3-bromopyruvate increases the cytotoxic effects of Chloroethylnitrosoureas to human glioma cells and the DNA interstrand cross-links formation. Toxicology. 2020;435:152413.
94. Chong J, Wishart DS, Xia J. Using metaboanalyst 4.0 for comprehensive and integrative metabolomics data analysis. Curr Protocols Bioinf. 2019;68(1):e86.

Publisher's note